SAE TECHNICAL PAPER 2012-01-1119

A sequential Chemical Kinetics-CFD-Chemical Kinetics methodology to predict HCCI combustion and main emissions

Bedoya I. D., Saxena S., Cadavid F. J., Dibble R. W., Aceves S.M., and Flowers D.L. "A sequential Chemical Kinetics-CFD-Chemical Kinetics methodology to predict HCCI combustion and main emissions". *SAE Paper 2012-01-1119*. doi:10.4271/2012-01-1119.

ABSTRACT

This study presents the development of a new HCCI simulation methodology. The proposed method is based on the sequential coupling of CFD analysis prior to autoignition, followed by multi-zone chemical kinetics analysis of the combustion process during the closed valve period. The methodology is divided into three steps: 1) a 1-zone chemical kinetic model (Chemkin Pro) is used to determine either the intake conditions at IVC to achieve a desired ignition timing or the ignition timing corresponding with given IVC conditions, 2) the ignition timing and IVC conditions are used as input parameters in a CFD model (Fluent 6.3) to calculate the charge temperature profile and mass distribution prior to autoignition, and 3) the temperature profile and mass distribution are fed into a multi-zone chemical kinetic model (Chemkin Pro) to determine the main combustion characteristics.

Different numbers of zones have been tested in the multi-zone step to determine the effectiveness of the general methodology. 40 zones are needed to achieve acceptable thermal stratification resolution to accurately predict peak heat release rates, peak pressures rise rates and ringing intensity. However, a simplified 12-zone reduced model is developed and validated to study combustion variables. Simulation results for the main combustion variables and emissions are compared with experimental results from a multi-cylinder HCCI engine fueled with biogas (60% CH_4 + 40% CO_2), and operating at different intake conditions. Comparisons between the proposed numerical methodology and experimental results show good agreement for power output (measured as $IMEP_g$), indicated efficiency, burn duration, peak pressure, individual ringing intensity, and HC and NO_x emissions. CO emissions are very sensitive to the input parameters of the 12-zone reduced model. However, when the peak temperature after ignition of boundary layer zones is properly handled; CO emissions are reasonably well predicted. According to the results, the methodology can successfully predict combustion parameters and emissions for HCCI engines in which the fuel and air are well mixed prior to ignition. Compared with previous sequential methodologies, the method proposed here allows for reduced number of zones, more uniform temperature profiles prior to ignition, more accurate estimation of mass located in each zone, reduced computing time and more accurate predictions of peak heat release rates, peak pressure rise rates, and ringing intensity.

INTRODUCTION

HCCI combustion has been extensively studied throughout the past decade as one option to meet the current and future engine emissions regulations while simultaneously achieving high efficiency. HCCI uses lower combustion temperatures causing lower NO_x emissions and premixed (or partially premixed) and dilute charge causing lower PM emissions. However, increases in CO and HC emissions are typical and must be addressed. Additionally, the absence of a direct ignition control method and reduced power output for HCCI engines are historically considered as disadvantages when compared to spark ignited and Diesel engines. To solve these problems, it is necessary to develop modeling tools that allow further understanding of the complex phenomena involved in the autoignition and combustion processes. This paper describes a new approach to predict HCCI combustion based on a sequential procedure using CFD and detailed chemical kinetics simulations.

Consensus has been gained from the pioneering study of Najt and Foster [1] on the necessity of including chemical kinetics to predict the autoignition event in HCCI mode. For a homogeneous charge, it is well accepted that single zone models combined with detailed chemical kinetics are able to predict the ignition timing when pressure, temperature and mixture composition are known. These models assume that the combustion chamber is a perfectly stirred reactor (having no spatial temperature and composition gradients);

however, this assumption limits the ability for predicting some combustion parameters (heat release rates, ringing intensity, CO and HC emissions) that are sensitive to spatial gradients. From previous experimental HCCI studies [2, 3] it has been shown that the ignition event is governed by radicals that appear almost instantaneously and are spatially distributed; therefore, combustion develops in absence of discernible flame propagation. During the combustion event, turbulence does not play an important effect since the chemical time is so short. However, turbulence indirectly influences the onset of combustion since it plays a role in determining the thermal stratifications that arise during the compression stroke because of heat transfer. According to the accepted theory of chemical and turbulence time scales, once ignition has occurred the burning rates are so fast that turbulence mixing rates cannot significantly affect the chemical reactions and heat release process. In fact, an estimate of time for H_2O_2 decomposition or local CO-to-CO_2 oxidation under HCCI conditions is on the order of 1-10 microseconds, while the turbulent time scales are on the order of 10 milliseconds for the integral length and timescale on the order of 1-100 microseconds for the Taylor micro-scale [4]. Thus, it can be concluded that combustion in an HCCI engine is governed by chemical kinetics, but fluid dynamics phenomena greatly influence temperature and species distribution prior to autoignition, and consequently, it has to be taken into account for accurate estimates of combustion parameters.

The small influence of turbulence during the combustion event in HCCI engines allows simplification of the models for prediction of ignition and combustion processes. The ideal model is one in which CFD and chemical kinetics calculations are fully integrated in every cell. However, this scheme is very expensive in computing time and usually it is only possible with simplified chemical kinetics mechanisms and coarse grids. Based on the importance of accounting for the influence of turbulence upon thermal stratifications and detailed chemical kinetics on combustion development, some co-authors of this paper proposed an alternative method to the fully coupled scheme. It was named the Sequential Fluid-Mechanic Chemical-Kinetic Multi-zone Model [5,6]. In this scheme the temperature and mass distribution before ignition were calculated with a CFD code (KIVA-3V). Then, the charge was divided into a relatively small number of zones (10) with different temperature histories and mass fractions, while the pressure and equivalence ratio was considered the same for all zones. Finally, a chemical kinetics code named HCT (Hydrodynamics, Chemistry and Transport) was run using the zonal distribution as input parameters. The numerical results were compared against experiments demonstrating good predictions of peak pressure, indicated efficiency, burn duration, and combustion efficiency. The HC emissions were under-predicted because of the low number of zones located in the crevices, and CO emissions were under-predicted because the mixing between zones was neglected during the calculations. In subsequent studies [7-9], the sequential multi-zone model was expanded to 40 zones to improve the predictions of CO and HC emissions without modeling the mixing between zones. HC emissions were generally well predicted, but the predictions of CO were not significantly improved. In an effort to improve accuracy, the mixing between zones was included in further modeling efforts by introducing a fully coupled CFD/multi-zone model in which the temperature, pressure and composition is calculated using the CFD code in each cell, while the chemical kinetics process is calculated only for 40 zones [10]. It was found that the there is a diffusion of fuel and CO from the boundary layer into the hottest zones that affects CO and HC emissions. Additionally, emission predictions were improved with respect to the original sequential multi-zone model. The sequential multi-zone approach has also been modified and applied to predict combustion variables under more complex conditions like these presented in PCCI engines, in which the charge composition is not uniform before ignition. The results show that the multi-zone model is able to predict burn duration and peak cylinder pressure with good accuracy [11]. Furthermore, this sequential approach has demonstrated accuracy and acceptable computational expense as compared with direct coupling of CFD and chemical kinetics to study PCCI combustion [12].

Despite the success of the fully coupled and sequential CFD/Multi-zone chemical kinetic model on the analysis of HCCI combustion, a better understanding of the effect of the number of zones on the charge temperature and mass distribution is necessary. These two important variables strongly influence ignition processes and heat release and thus it is important to understand the balance between accuracy versus computing time as the number of zones is increased. The aim of this paper is to present a 12-zone reduced model to study HCCI combustion allowing accurate predictions of combustion variables and reduced computing time, based on the Sequential Fluid-Mechanic Chemical-Kinetic Multi-zone Model proposed and improved by some co-authors [5,6]. Fluent 6.3 is used in the CFD calculations and Chemkin Pro is used as the chemical kinetics solver.

METHODOLOGY

The numerical approach is a sequential chemical kinetic-fluid mechanic-chemical kinetic model to predict HCCI combustion variables during the closed valve period. The model follows three steps: 1) The 1-zone model of Chemkin Pro is used to predict the IVC conditions that cause a desired ignition timing, or the ignition timing that results from prescribed IVC conditions, 2) These initial conditions at IVC and ignition timing are used as inputs for Fluent 6.3, which determines the in-cylinder temperature profiles and mass distribution prior to autoignition, and 3) The time dependent temperature and mass distributions given by Fluent 6.3 are fed into the multi-zone-model of Chemkin Pro, which predicts main combustion variables. Each step of the methodology is described in detail in the following sections.

DETERMINING CONDITIONS AT IVC, CRANK ANGLE AT IGNITION, AND ENERGY SWITCH CRANK ANGLE

The calculation of combustion variables during the closed valve period requires the determination of the pressure, temperature, and mass stratification at IVC. This is not trivial because many variables are involved in the calculation of the initial conditions at IVC, such as heat transfer during induction, mixing of the charge with trapped exhaust gases, and pressure drop due to wall friction, among others. Simulating the intake stroke can give a good approximation of the initial conditions at IVC; however, an accurate estimation is still difficult for all possible engine configurations and operating conditions. Since the subject of this research is modeling the closed valve period, the simulation of the full cycle will be explored in future research.

The 1-zone model accompanied by detailed chemical kinetics has shown to be a reliable method to predict the igniting time in HCCI engines because it accurately predicts the temperature history of the hottest core zone of the charge before ignition [12]. Chemkin Pro´s 1-zone model determines the ignition timing for given IVC conditions or the IVC conditions leading to desired ignition timing. This new step has been incorporated before the traditional sequential CFD/chemical kinetics approach because of the following advantages:

- Determination of practical operating limits before CFD simulations: As noted in previous research, the ignition timing plays an important role on the load limits and cyclic variations of HCCI engines, with the optimum ignition crank angle (CA10) interval approximately located between TDC and 5 CAD aTDC (depending on the fuel) [14,15]. Usually if ignition occurs before TDC, the pressure rise rates are so high that excessive ringing intensities are encountered and the engine can be damaged. On the other hand, if ignition occurs very late, the cyclic variability is increased leading to lower power output and lower indicated efficiency, as well as higher CO and HC emissions (and eventually complete misfire). The 1-zone model allows for parametric studies involving important factors like compression ratio, charge composition, initial pressure and temperature. Therefore, knowing the ignition timing for a given combination of these factors is useful to save time in CFD/multi-zone chemical kinetics calculations for operating conditions that are not practical for HCCI operation.

- Energy switch crank angle determination before multi-zone simulations: The energy switch crank angle represents the time when the temperature profile from the CFD calculations are abandoned and the detailed chemical kinetics are adopted in the multi-zone model of Chemkin Pro. If too early a switch angle is selected, the effects of turbulence on thermal stratification (captured in the CFD analysis) are lost and the heat transfer to the walls is determined less accurately, increasing uncertainty of the ignition timing. On the other hand, when the switch angle is excessively delayed, the early chemical kinetics is not captured. This also causes errors in the ignition timing. In this research, it is found that the energy switch crank angle strongly influences ignition timing; therefore, a good prediction of this parameter is necessary prior to multi-zone calculations.

The 1-zone model simulations include detailed chemical kinetic calculations. Since the methodology is validated against experimental data for methane and carbon dioxide (60% CH_4 + 40% CO_2 on a volumetric basis), the GRI-Mech 3.0 [16] is used as the gas phase reaction mechanism. GRI-Mech 3.0 considers 53 species and 325 reactions and has been optimized for a temperature range of 1000-2500 K, a pressure range of 10 Torr-10 atm, and equivalence ratios from 0.1 to 5 in premixed systems [16]. Since the autoignition temperature of methane is above 1000 K, the peak combustion temperature is typically lower than 2000 K, and the tested equivalence ratios were between 0.19 and 0.29, GRI-Mech 3.0 is an appropriate mechanism to use in this study. The peak in-cylinder pressures are expected to be higher than the recommended range (10 Torr – 10 atm), but a previous research [17] has validated the accuracy of GRI-Mech to predict methane auto-ignition through shock tube experiments at high pressures (40-250 atm) and intermediate-to-high temperatures (1040-1500 K). Furthermore, other studies have validated a previous version of this mechanism (GRI-Mech 2.1) under Diesel like conditions for direct injection of natural gas [18,19]. The specified initial pressure at IVC is set such that the predicted peak pressures matches the peak pressure from the experiments at motored conditions. Equivalence ratios are calculated using exhaust gas analysis from experimental data. Wall temperature is specified as a function of equivalence ratio according to a published methodology [20].

Heat transfer to the cylinder walls is estimated with the Woschni correlation [21] including recommended modifications for HCCI combustion [22, 23]. The global heat transfer coefficient is calculated as follows:

$$h_{global} = C_0 3.28 B^{-0.2} p^{0.8} T^{-0.73} v_{tuned}^{0.8} \quad (1)$$

$$C_0 = 0.65$$

Where h_{global} is the heat transfer coefficient of the gas boundary layer (W/m^{2}K), C_0 is a factor used to match the peak of the experimental heat transfer, B is the bore (m), p is the instantaneous in-cylinder pressure (kPa), T is the instantaneous in-cylinder temperature (K), and v_{tuned} is the instantaneous characteristic velocity (m/s). v_{tuned} was calculated as follows:

$$v_{tuned} = C_1 \overline{S}_p + \frac{C_2}{6} \frac{V_d T_i}{p_i V_i} (p - p_{motored}) \quad (2)$$

Where C_1 and C_2 are constants depending of the engine type, S_p is mean piston speed (m/s), V_d is the swept volume (m^3), T_i, p_i, and V_i are the initial temperature, pressure and volume at IVC (1-zone simulations) and -50 CAD aTDC (multi-zone simulations), and $p_{motored}$ is the calculated instantaneous motored pressure (kPa). The following values were used for the constants in Eq. (2):

$$C_1 = 2.28 + C_3 \frac{v_{swirl}}{\overline{S}_p}; \quad C_2 = 3.24 * 10^{-3}; \quad C_3 = 0.308$$

$$\frac{v_{swirl}}{\overline{S}_p} \approx 2$$

The experiments were conducted in the Combustion Analysis Laboratory, at the University of California, Berkeley. A 1.9L Volkswagen TDI Diesel engine adapted for HCCI operation was run with biogas. Details about the experimental methodology can be found in recent publications [24, 25]. Table 1 shows the engine specifications.

Table 1 – Technical engine specifications.

Designation	VW TDI, four stroke, four cylinders, water cooled, diesel engine
Firing order	1-3-4-2
Original charge aspiration	Turbocharged
Modified charge aspiration	Supercharged and heated
Displacement	1890cm^3
Original Compression ratio	19.5 : 1
Modified compression ratio	16.86
Bore x stroke	79.5 x 95.5 mm
Connecting rod length	144.0 mm
Valves (intake, exhaust)	1, 1
Intake valve open (IVO)	16 CAD aTDC
Intake valve close (IVC)	25 CAD aBDC
Exhaust valve open (EVO)	28 CAD bBDC
Exhaust valve close (EVC)	19 CAD aTDC
Original rated power	60 kW at 3300 rpm
Original maximum torque	210 Nm at 1800 rpm
Engine speed during the experiments	1800 rpm
Original combustion chamber	Bowl
Modified combustion chamber	Hemispherical/shallow bowl
Fuel composition, volumetric basis	60% CH_4 + 40% CO_2

The crank angle of ignition is defined as the crank angle for the peak molar fraction of H_2O_2, which usually coincides with the crank angle of 10% of cumulative heat release (CA10) in the simulations. For fuels with low temperature heat release, i.e. Diesel fuels, the CA10 point tends to be earlier than the H_2O_2 peak. Therefore, these fuels require a modified definition of ignition timing to reduce the

uncertainty in temperature at IVC and energy switch crank angle. Figure 1 shows the 1-zone model results for the normalized H_2O_2 molar fraction and the normalized cumulative heat release using two equivalence ratios, intake pressure of 2.2 bar, and intake temperature of 483 K. The calculated results capture the trends observed during the experiments in which the ignition timing was advanced when the equivalence ratio was increased from ϕ=0.19 to ϕ=0.29. The temperature at IVC for ϕ=0.19 is expected to be lower (463 K) than for ϕ=0.29 (478 K) because of the increased heat transfer during the induction stroke for leaner charges at a fixed intake temperature. Other factors affecting the temperature at IVC like heating by the residual gases are minor because neither internal nor external EGR was used during the experiments, the exhaust backpressure was reduced because the turbocharger was removed, and the valve overlap period is very short (3 CAD). The higher temperature at IVC leads to higher temperature at TDC and early population of H_2O_2 radicals before TDC which cause fuel autoignition.

As mentioned before, the 1-zone model is also used to estimate energy switch crank angles as inputs for multi-zone calculations. Previous studies using the sequential CFD/Chemical kinetics approach have shown that the ignition timing is properly predicted during multi-zone simulations without taking into account the intermediates/radicals formed during compression stroke prior the switch crank angle if no significant heat release takes place and the temperature at IVC is properly adjusted [5,6]. In the methodology proposed here, the temperature at IVC allowing a specific crank angle at ignition is calculated before CFD and multi-zone calculations as well as the switch crank angle allowing for no significant heat release prior the beginning of multi-zone chemical kinetics calculations. Therefore, the effect of intermediate/radicals formed during compression stroke (previous to the switch crank angle) on ignition timing is expected to be negligible. Provided that rapid H_2O_2 breakdown triggers ignition in HCCI engines, the initial energy switch crank angle was estimated at 1 CAD before the crank angle for the peak molar concentration of H_2O_2. Parametric studies on the effects of the switch angle over the predicted ignition timing were performed with multi-zone simulations for cases shown in Fig.1. A range of 10-0 CAD bTDC was tested for the energy switch crank angle, finding that earlier switching tends to advance the onset of combustion. Since the best matching of the experimental crank angle at ignition was achieved using the initial criterion, 1 CAD before H_2O_2 molar peak is used as the recommended energy switch crank angle for all tested cases.

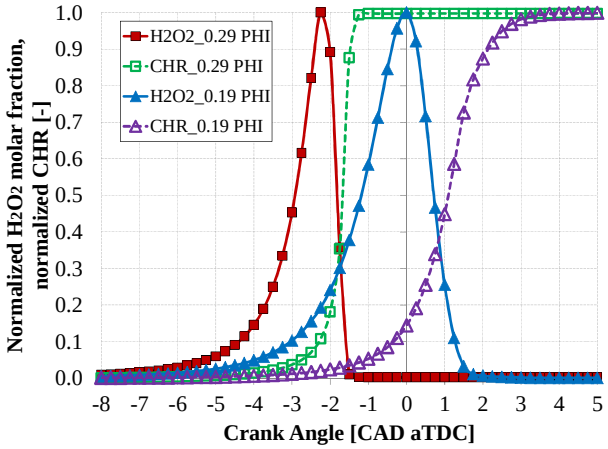

Figure 1- Normalized H_2O_2 molar fraction, and normalized cumulative heat release (CHR) for ϕ=0.29 and ϕ=0.21. P_{IVC}=2 bar, T_{IVC} for ϕ=0.29 is 478K, T_{IVC} for ϕ=0.19 is 463K.

As previously mentioned, Chemkin Pro´s 1-zone model allows for parametric studies that simplify the process of estimating the initial conditions at IVC for HCCI operation. Figure 2 presents the simulated results of crank angle at ignition related with the temperature at IVC for three equivalence ratios. The experimental ignition timings (represented with not filled markers) were estimated by averaging 300 consecutive cycles for five different replicas for each equivalence ratio. The simulations show that for a given temperature at IVC, the ignition timing is advanced for lower equivalence ratios. This occurs because of the higher charge temperatures caused by higher specific heat ratios with leaner mixtures. In the experiments, the temperature at IVC and wall temperatures tend to increase with equivalence ratio; thus, ignition timing advances as the equivalence ratio increases (Fig. 2). It is evident that without the help of the experimental results it is difficult to estimate the temperatures at IVC. This limitation will be addressed in future research by modeling the full cycle (including gas exchange processes).

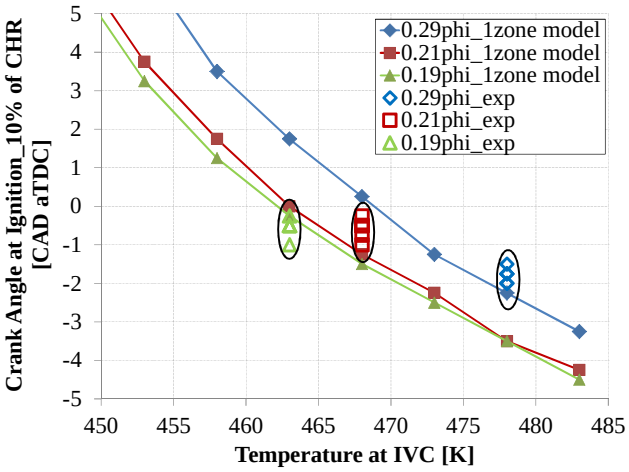

Figure 2 – Simulated and experimental ignition timing vs. temperature at IVC. P_{IVC}=2bar, T_{INT}=483K.

TEMPERATURE AND MASS DISTRIBUTION CALCULATION PRIOR TO AUTOIGNITION

Fluent 6.3 is used as the CFD code in the following stage of the calculation methodology. Given that the piston´s head used during the experiments is fully symmetrical, a 2D axisymmetric configuration was chosen to predict the flow patterns. Fluent simulations use the pressure-based segregated implicit solver with the PISO (Pressure-Implicit with Splitting of Operators) algorithm for the pressure–velocity coupling, the PRESTO (Pressure Staggering Option) scheme for pressure, and the second order upwind discretization for density, momentum, swirl velocity, turbulent kinetic energy, turbulent dissipation rate, and species. 2D axisymmetric simulations are run from IVC until 10 CAD aTDC assuming a motored cycle. The pressure and temperature at IVC from the 1-zone model are used at the beginning of the CFD model assuming homogeneous temperature and charge composition at IVC. The wall temperatures are calculated using a methodology [20] which correlates the surface temperatures with equivalence ratio. Typical values of 453K, 413K, and 385K are used for the piston surface, cylinder head, and cylinder wall respectively. Turbulence is modeled with the standard κ-ε model using standard wall functions and default inputs given by the code. The flow pattern is initialized at IVC assuming the turbulence intensity (10%) and the swirl ratio (2) for all simulations.

The base grid for this study has been built in Gambit 2.2 and includes 3,672 cells at TDC (Figure 3) and 15,422 at IVC. The grid has been refined near the walls in the axial and radial direction for better prediction of mass and temperature in the boundary layer and crevice regions. The radial cell length in the crevices is 50 µm, allowing 5 cells in the ring crevice, while the radial cell length in the core of the combustion chamber is between 0.25 and 0.5 mm approximately.

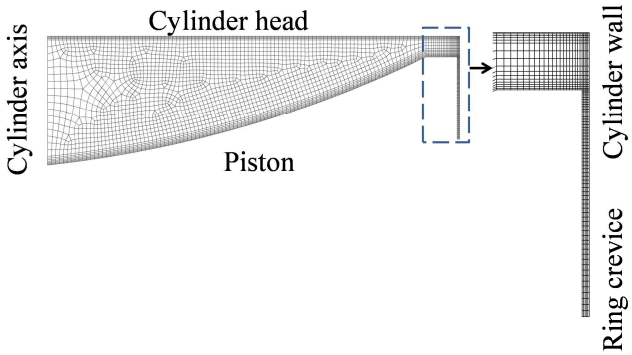

Figure 3 – Full view of the base grid at TDC and zoomed view of wall boundary layer and ring crevice.

Two additional grids have been built to perform a sensitivity study on the effects of mesh resolution over the predicted in-cylinder average temperature at motored conditions from IVC to EVO. The cell length and height were kept around 50 µm near the walls. The details for each mesh resolution are given in Table 2.

Table 2 - Different grid schemes tested for sensitivity.

Grid identification	Total cells at TDC	Total cells at IVC	Time step (CAD)
Grid #1 (base)	3,672	15,422	0.25
Grid #2	6,018	32,418	0.25
Grid #3	32,600	107,330	0.25

Figure 4 shows the simulated average temperature traces achieved for the different grid schemes described in Table 2 without volumetric reactions. The initial pressure at IVC is corrected to match the experimental peak pressure at motored conditions. From Fig. 4 it can be observed that the predicted average temperature traces are weakly affected by the grid scheme; therefore, the base grid was selected because it produces accurate results and has the lowest computing time.

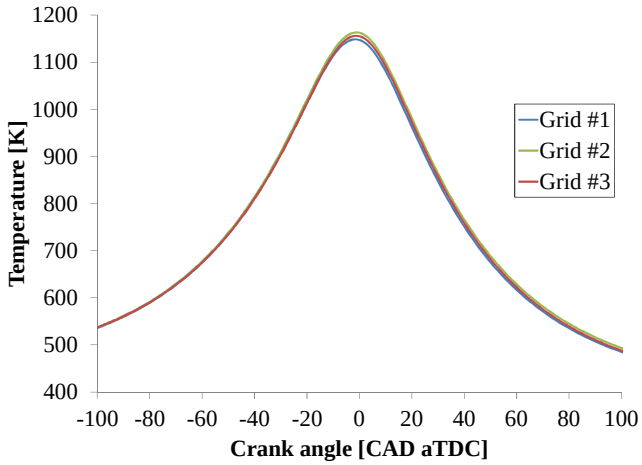

Figure 4 – Simulated average in-cylinder temperature traces at motored conditions for three different grid schemes. P_{IVC}=2bar, T_{IVC}=478K, ϕ=0.29.

Once the CFD simulations were finished, the next step is the calculation of the temperature and mass fraction profile for a range of -50 CAD aTDC to 10 CAD aTDC. This stage comprises three sub-stages: 1) Definition of number of zones according to charge temperature distribution, 2) Calculation of the zone temperature limits and zone average temperature, and 3) Calculation of the mass distribution and zone average mass fraction.

Defining the number of zones and zone average temperatures

Using a large number of zones allows accurate results, at the expense of long computing time. The 1-zone simulation takes 1-5 minutes, the CFD simulations takes about 1 hour (base grid and 0.25 CAD time step), and the multi-zone simulations take about 30 minutes (40 zones and 0.25 CAD time step). All computations are run on a 2.7 GHz single processor workstation.

Grouping a specific number of cells to form a zone represented by an averaged cell temperature depends on the lower and upper temperature limits of the grouped cells. In a similar way, these limits are affected by the overall temperature distribution of the charge at a specific time. Previous research [5,6] has shown that when KIVA-3V is used as the CFD code, 10 zones give enough resolution to accurately predict main combustion variables (like IMEP, combustion efficiency, and indicated efficiency). However, 40 zones are necessary for acceptable prediction of HC emissions [7-9], and 40 zones accompanied with simulation of mixing between zones are needed for reasonably predicting CO emissions [10]. The effect of the number of zones on the prediction of peak pressure rise rates and ringing intensity has not been studied in detail in the HCCI literature, and this topic is discussed below in the section on multi-zone chemical kinetics.

This paper shows a parametric study of the effect of the number of zones on the temperature distribution. The number of zones is defined using the post-processor tool of Fluent 6.3, which also provides the temperature limits for each zone. Figure 5 shows the temperature contour for 10 zones at -3 CAD aTDC. Each temperature interval in the color map identifies a specific zone. Zones 1-4 are in the main crevice, zones 5-7 are part in the boundary layer and part in the crevices, zone 8 is the boundary layer, zone 9 is in the boundary layer and in the core, and zone 10 is in the core of the combustion chamber. As noted in the color map the difference between the lower and upper temperature limits for each zone is around 65 K, which is large considering the strong dependence of chemical kinetics on charge temperature. A non-representative average temperature caused by an insufficient number of zones leads to erroneous predictions of the average heat release rates in the hottest zones. The method will underpredict reactivity of hotter parts of the zone and overpredict reactivity of colder parts. Therefore, a larger number of zones is needed for better prediction of pressure rise rates.

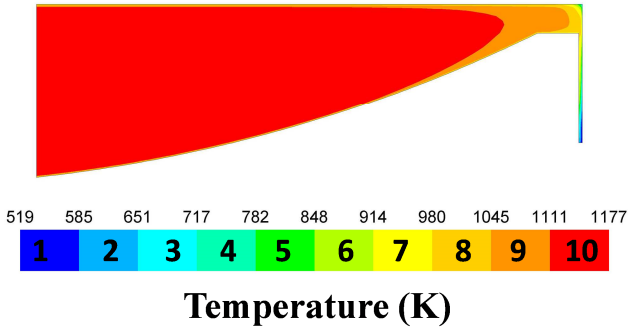

Figure 5 – Temperature distribution for 10 zones at -3 CAD aTDC. P_{IVC}=2bar, T_{IVC}=478K, ϕ=0.29.

Two additional multi-zone simulations, with 20 and 40 zones, were tested to study the effect of resolution on the average zone temperature. As expected from the uniform temperature distribution shown in Fig. 5, when the number of zones is increased the difference between the average zone temperatures of consecutive zones is uniformly reduced. For a specific number of zones, the difference between the lower and upper temperature limits is almost constant throughout the charge. In Fig. 6, these trends are shown for the 10 hottest zones related with the number of zones at -3 CAD aTDC. According to the information presented in Fig. 6, 40 zones allow a good resolution with the difference between average zone temperature in neighboring zones being around 16 K. In this case, the average zone temperature is within ±8K of the maximum and minimum temperature within each zone. Similar results were achieved for the entire crank angle interval between -50 CAD aTDC to 10 CAD aTDC.

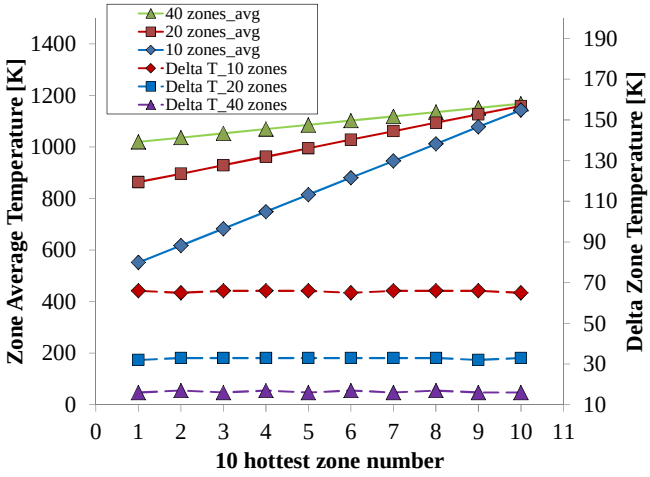

Figure 6 – Average zone temperature and Delta zone temperature (Tmax-Tmin) at -3 CAD aTDC for the 10 hottest zones of three different numbers of zones. P_{IVC}=2bar, T_{IVC}=478K, ϕ=0.29.

Calculating the mass fraction distribution as a function of the number of zones

The mass fraction for each zone represents the fraction of the charge with temperatures between the lower and upper zone temperature limits. The mass for each cell is calculated as follow:

$$m_{cell} = V_{1R\,cell} * \rho_{cell} * 2\pi \qquad (3)$$

Where m_{cell} (kg) is the mass of each cell, $V_{1R\ cell}$ (m^3) is the cell volume using a reference depth of 1 radian, and ρ_{cell} (kg/m^3) is the cell density. Once the mass is calculated for all cells, the zone mass fraction is determined by adding the mass of cells within the zone temperature interval and dividing the result by the total mass of the charge. Figure 7 shows the zone mass fraction related with the average zone temperature for the 10 hottest zones at -3 CAD aTDC and for different total numbers of zones. The mass fraction in the core is strongly affected by the number of zones while the mass fraction in the crevices is insensitive to the numbers of zones. When the charge is divided in 10 zones the mass fraction in the hottest zone is close to 80%; therefore, almost all the fuel is expected to be ignited at same time and burned at the same rate during the main heat release event.

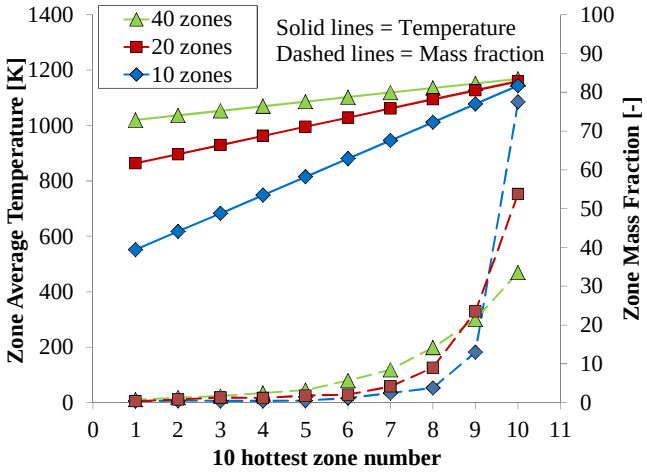

Figure 7 – Average zone temperature and zone mass fraction at -3 CAD aTDC for the 10 hottest zones of three different numbers of zones. P_{IVC}=2bar, TIVC=478K, ϕ=0.29.

Defining the time-dependent temperature and mass fraction profiles

Once the average temperature and mass fraction distribution are defined for each crank angle, the temperature and mass fraction profiles are built between -50 CAD aTDC and 1 CAD before the ignition timing previously defined by the 1-zone model. Figure 8 (a) shows a temperature profile for a 10 zone model. The difference between the average zone temperatures for consecutive zones is almost constant through the charge at a specific crank angle. This trend makes the profile highly uniform. The temperature range covered by the coldest zones (1-5) is similar to the temperature range covered by the hottest zones (6-10). These trends suggest that the temperature distribution is not dependent on the mass distribution provided that practically all the charge is located in the hottest zones, but the thermal distribution is uniform through the charge. In Fig. 8(b) the average zone temperatures for zones 1-9 are presented as a function of the average temperature in zone 10. As shown in the figure, the average temperature history for different zones can be modeled from the average temperature history in the hottest zone by using a linear regression. Similar results were achieved for 20 and 40 zones. This theoretical assumption can make it easier to determine the thermal stratification using the temperature history calculated from the 1-zone model for the hottest zone in the charge.

The temperature profiles (Figure 8b) differ from those achieved with KIVA-3V for 10 zones (Figure 8c) [5, 6], in which zones 1-5 covers a higher range of temperature than zones 6-10, the three hottest zones are almost isothermal, and the gap between the average zone temperature for consecutive zones considerably increases for the coldest zones (Figure 8c). These differences become smaller when the number of zones is increased; however, some differences remain and these can be important for predictions of most sensitive variables or when combined with high levels of species in-homogeneities as in PCCI engines. Since many factors can affect the charge temperature distribution, a direct comparison between both CFD codes is not possible at this point. It will be addressed in future research.

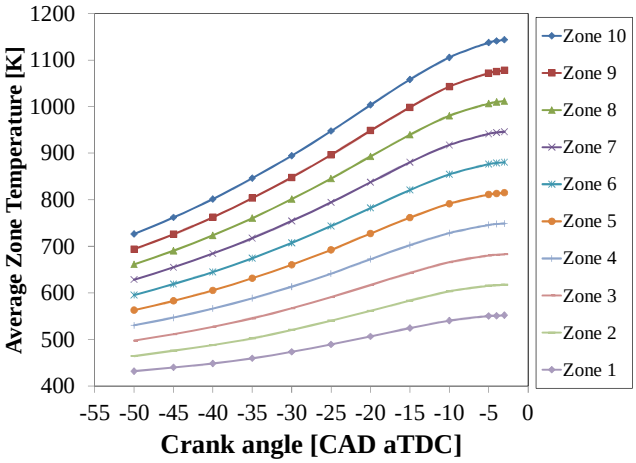
Average Zone Temperature [K]
1200
1100
1000
900
800
700
600
500
400
-55 -50 -45 -40 -35 -30 -25 -20 -15 -10 -5 0
Crank angle [CAD aTDC]
Zone 10
Zone 9
Zone 8
Zone 7
Zone 6
Zone 5
Zone 4
Zone 3
Zone 2
Zone 1

(a)

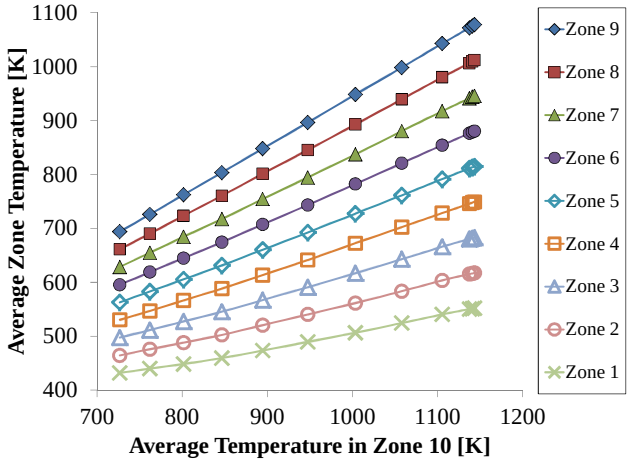
Average Zone Temperature [K]
1100
1000
900
800
700
600
500
400
700 800 900 1000 1100 1200
Average Temperature in Zone 10 [K]
Zone 9
Zone 8
Zone 7
Zone 6
Zone 5
Zone 4
Zone 3
Zone 2
Zone 1

(b)

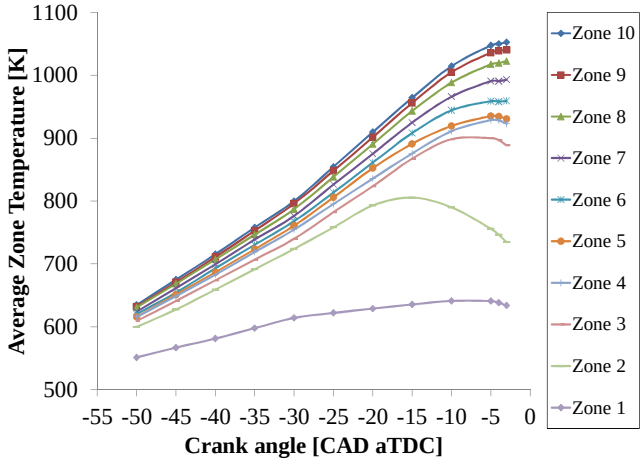
Average Zone Temperature [K]
1100
1000
900
800
700
600
500
-55 -50 -45 -40 -35 -30 -25 -20 -15 -10 -5 0
Crank angle [CAD aTDC]
Zone 10
Zone 9
Zone 8
Zone 7
Zone 6
Zone 5
Zone 4
Zone 3
Zone 2
Zone 1

(c)

Figure 8 – (a) Average zone temperature profile for a 10 zones distribution. (b) Average zone temperature in zones 1-9 related with the average zone temperature in zone 10. P_{IVC}=2bar, T_{IVC}=478K, ϕ=0.29. (c) Average zone temperature profile for a 10 zone distribution calculated with KIVA-3V, adapted from [5].

The zone mass fraction presents slight differences with time for zones located in the boundary layer and crevices (not shown), these differences are higher for zones located in the core of the charge, but tend to be minimized when the number of zones is increased. Since the amount of mass in the hottest zones affects the heat release rates, the mass fraction distribution close to the crank angle at ignition is used instead of time average mass fractions.

MULTI-ZONE CHEMICAL KINETICS AND REDUCTION OF THE NUMBER OF ZONES

The final step of the numerical methodology is running Chemkin Pro's multi-zone model using the temperature and mass profiles found in the previous stage. During the compression stroke, the temperature profiles are followed without accounting for chemical kinetics in the calculation. The chemical kinetic calculations are activated at the energy switch crank angle, which represents the time when heat release becomes important. The model assumes that zones are perfectly stirred reactors with different temperature and mass fractions, but with the same equivalence ratio and pressure. Mechanical work between zones is their only interaction; mixing, diffusion, and heat transfer between zones are neglected. During combustion, wall heat transfer is calculated using the Woschni correlation as mentioned for the 1-zone model and heat loss from each zone is estimated by setting a parameter named External Heat Transfer Area Fraction (EHTAF). The initial pressure is slightly adjusted to match the experimental pressure trace at 50 CAD bTDC.

The effect of the number of zones is first studied. Figure 9(a) shows the in-cylinder pressure traces and Fig. 9(b) shows the apparent gross heat release rate (GHRR) for the different number of zones compared with experimental traces running at ϕ=0.29. The heat release and pressure rise rates are over predicted when 10 and 20 zones are used because a large fraction of the fuel (78% for 10 zones and 56% for 20 zones) is suddenly burned once the ignition event begins. A 40-zone model captures the thermal charge stratification with enough resolution to improve the predictions of the heat release rates and consequently the pressure rise rates, which are necessary to determine the ringing intensity and high load limits. Consequently, the temperature profiles and mass fraction distribution provided by the 40-zone model is used in the following step of the methodology.

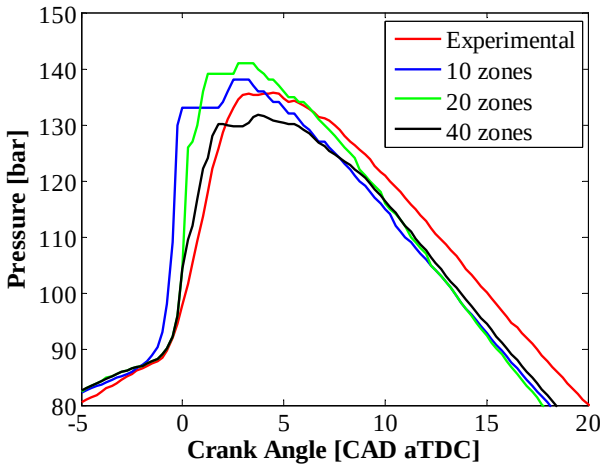

(a)

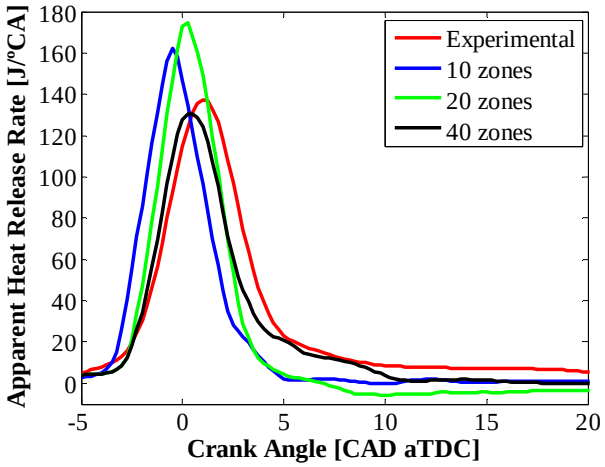

(b)

Figure 9 – (a) Simulated and experimental pressure traces. (b) Simulated and experimental apparent gross heat release rates. P_{IVC}=2bar, T_{IVC}=478K, ϕ=0.29.

Reducing the number of zones

According to the results in Fig. 9(a) - (b), the average zone temperatures estimated using 10 and 20 zones tend to be non-representative of the charge in each zone. This problem is easily solved by increasing the number of zones to 40. However, this increases the computational time. The 40-zone model allows good resolution in the hottest zones to calculate the main heat release and in the coldest zones for a better estimation of HC emissions. Provided that the coldest zones do not react through the combustion process, the number of zones can be reduced by grouping the non-reacted zones into a single zone without affecting the main heat release event. The location of the non-reacted zones is determined by running simulations assuming adiabatic conditions during the multi-zone chemical kinetic simulation step at the highest intake temperature. For a 40 zone distribution only the mass located in the 11 hottest zones is burned during combustion as shown in Fig. 10. Zones 1-27 are not shown because they are colder than zone 28.

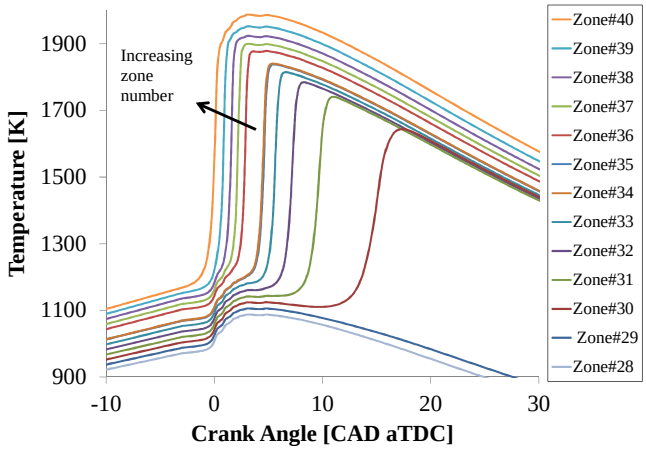

Figure 10 – Temperature history for zones 28-40 at adiabatic conditions. P_{IVC}=2bar, T_{IVC}=478K, ϕ=0.29.

According to Fig. 10, zone 29 represents the spatial threshold of the charge located mainly in the crevices which is the main source of HC emissions. It is expected that zones 1-29 will remain unburned when heat loss is accounted for in the energy balance; thus, these zones are grouped into a single zone, reducing the 40-zone model to a 12- zone model. The new model preserves the resolution of the temperature and mass distribution in the hottest zones, and significantly reduces the time to run multi-zone simulations (by around 50%). It must be noted that the number of zones of the reduced model can change with multiple factors. For the fuel and test conditions in this research, 11 zones are finally devoted to the core of the combustion chamber and the boundary layer. Zone 12 is the hottest and follows the temperature profile and mass fraction calculated for zone 40, zone 11 follows the temperature profile and mass fraction calculated for zone 39, and so on until zone 2 which follows the temperature profile and mass fraction estimated for zone 30. Zone 1 is the coldest and follows the temperature profile calculated for zone 29 (to preserve the difference between zone average temperatures), and the cumulative mass fraction from zones 1-29 in the 40 zone distribution. Table 3 shows the mass fraction within the zones.

Table 3 – Mass fraction distribution for the 12-reduced zones model

Zone number	Mass fraction (%)
12	33.6
11	21.4
10	14.1
9	8.5
8	5.6
7	3.2
6	2.5
5	1.7
4	1.2
3	0.7
2	0.9
1	6.6

METHODOLOGY VALIDATION

The simulation methodology has been validated against experimental results from the VW TDI engine (Table 1). Six different experimental cases have been selected. Cases 1-3 explore changes in power output (varying equivalence ratio) at constant intake pressure and temperature, and cases 4-6 capture changes in combustion phasing (varying intake temperature) at constant equivalence ratio and intake pressure. Table 4 shows the experimental results for the six selected cases. The experiments have been described in previous publications [24, 25], and reported values represent 300 cycle averages. Ringing intensity is calculated using the method developed by Eng [26].

Table 4 – Average experimental results over 300 cycles for biogas as fuel (60% CH_4 + 40%CO_2 in a volumetric basis).

Variable/Case	C1	C2	C3	C4	C5	C6
Equivalence ratio (ϕ)	0.19	0.21	0.29	0.33	0.33	0.33
[1]Inlet temperature (K)	483	483	483	460	453	448
Inlet pressure (bar abs)	2.2	2.2	2.2	2.2	2.2	2.2
$IMEP_g$ (bar)	3.8	4.8	7.1	7.5	8.7	8
Normalized standard deviation of $IMEP_g$ (%)	12.6	5.8	2.1	2.6	2.9	20
Gross Indicated efficiency (%)	37	38	42	40	42	38.5
Average ringing intensity (MW/m^2)	1.2	3.2	21.9	18.7	12	6.3
[2]Individual ringing intensity (MW/m^2)	4.9	8.64	23	23.5	16	5.3
[3]Burn duration (CAD)	15	14.5	10.5	8.5	11.5	15
[4]HC emissions (ppm C)	2867	2658	2475	3585	3707	5852
CO emissions (ppm)	2848	2564	2018	2290	2130	2443
NO_x emissions (ppm)	0.56	0.59	13.3	37	9.8	4.8

[1] Measured at the intake manifold.

[2] Individual ringing intensity is calculated using a representative cycle instead of averaging 300 cycles.

[3] Burn duration is calculated as the crank angle difference for points given 10% of the apparent peak gross heat release rate.

[4]Exhaust emissions were measured in the exhaust manifold

The experimental pressure traces that are analyzed are the average of 10 representative cycles located in a window of ±10% of the average $IMEP_g$ and the highest individual ringing intensity calculated for 300 cycles. The average experimental pressure trace from 300 cycles is not used to compare with simulated pressure traces because the peak pressure rise rates tend to be underpredicted when cyclic variability is increased. The multi-zone model does not account for cyclic variations. Both experimental and calculated traces have been filtered with a Savitzky-Golay smoothing filter [27] to allow for more accurate analysis of the pressure rise rates.

In the multi-zone model of Chemkin Pro the fraction of the effective surface area for heat transfer from each zone to the walls is assigned by setting the EHTAF. Defining a criterion to assign this parameter to each zone is difficult because the heat transfer between zones is not included in the model; therefore, a parametric study was performed applying different heat transfer schemes in the 12-zone reduced model. These schemes were: EHT1= adiabatic, EHT2= three hottest zones adiabatic, EHT3= uniform EHTAF in all zones (8.33%), EHT4= EHTAF proportional to the mass fraction in all zones. Table 5 shows the EHTAF for each zone in the parametric study. The sum of the EHTAFs is equal to 100%, except for the adiabatic case.

Table 5 – External Heat Transfer Area Fraction within the 12-reduced zones model followed in the parametric study for heat transfer schemes

External Heat Transfer Area Fraction (%) as function of the Heat transfer scheme				
Zone	EHT1	EHT2	EHT3	EHT4
12	0	0	8.3	33.6
11		0		21.4
10		0		14.1
9		30		8.5
8		20		5.6
7		6.5		3.2
6		4.5		2.5
5		3		1.7
4		1.5		1.2
3		0.75		0.7
2		0.25		0.9

1		33.5		6.6

It is important to note that the EHTAF approach only influences the results starting from the energy switch crank angle. Prior to this time, heat transfer is calculated in more detail in the CFD step and captured in the temperature profiles which are used as inputs to the multi-zone model. Case 3 (in Table 4) has been selected to illustrate the effects of the heat transfer scheme on the calculated pressure development because its cycle-to-cycle variation is the lowest. Figure 11(a) shows experimental and simulated pressure traces for Case 3 and the tested heat transfer schemes and Fig. 11(b) shows the ratio of calculated to experimental results for combustion variables using different heat transfer schemes. The agreement in the peak pressure when comparing experimental and numerical pressure traces (with heat transfer enabled) is close to 95% and the shape before the peak pressure is almost identical. The differences between the calculated pressure traces in which heat transfer has been considered are not significant; therefore the calculated $IMEP_g$ and the indicated efficiency are not highly affected by the heat transfer scheme in these cases, as shown in Fig. 11(b). The best pressure trace prediction is achieved for adiabatic combustion; however, the $IMEP_g$ and the indicated efficiencies are over-predicted for Case 3 (Fig. 11(b)). Similar trends were observed for the rest of cases. For Case 3, the best overall agreement between calculated and experimental results was observed when the three hottest zones (10-12) were considered adiabatic (EHT2) and the EHTAF was considered as proportional to the mass fraction present in the other zones (1-9, Fig. 11b). Similar trends were observed for the rest of cases. In subsequent analysis, the simulated results use the EHT2 scheme.

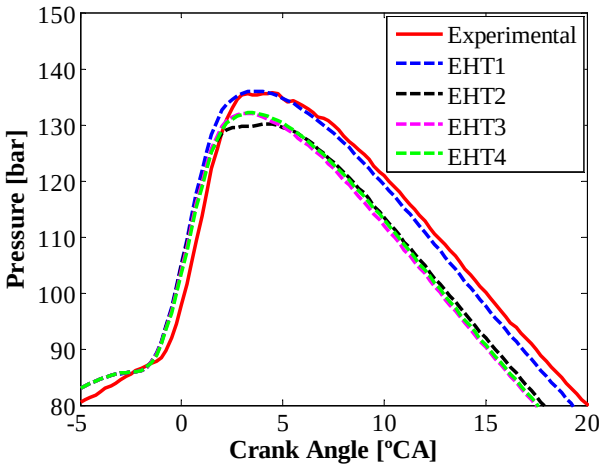

(a)

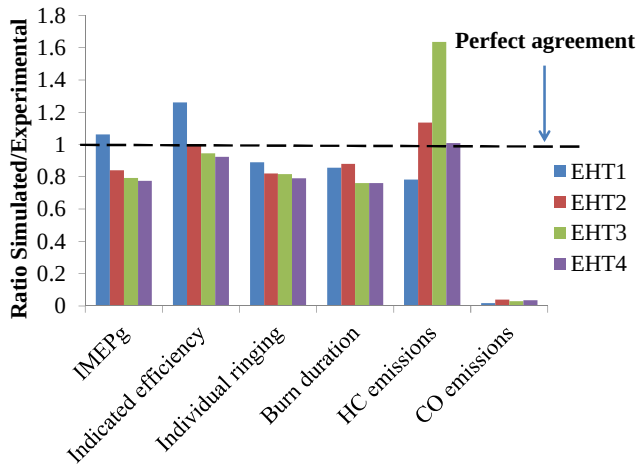

(b)

Figure 11 – (a) Comparison between the simulated pressure traces using different heat transfer schemes (EHT1-EHT4) and the experimental pressure trace for Case 3 (C3). (b) Simulated-over-experimental results ratio for Case 3 using different heat transfer schemes (EHT1-EHT4). Experimental results are extracted from Table 3. Calculated HC and CO emissions are located at EVO.

Cases 1-3 are representative of the varying load conditions for the tested fuel: Case 1 represents a low load case ($IMEP_g$ = 3.8 bar) with high cyclic variability (normalized standard deviation of $IMEP_g$ = 12.6%), Case 3 represents a high load case ($IMEP_g$ = 7.1 bar) and highest average ringing intensity (21.9 MW/m^2). Figure 12 shows a comparison between simulated and experimental pressure traces. The 12-zone model allows good prediction of the rate of pressure rise when higher equivalence ratios are used, and the agreement with experimental peak pressures is within 95-98%. The differences between the traces for Case 3 may be caused by slight errors in experimental equivalence ratio, and difficulties in controlling the intake temperature and pressure for multi-cylinder operation.

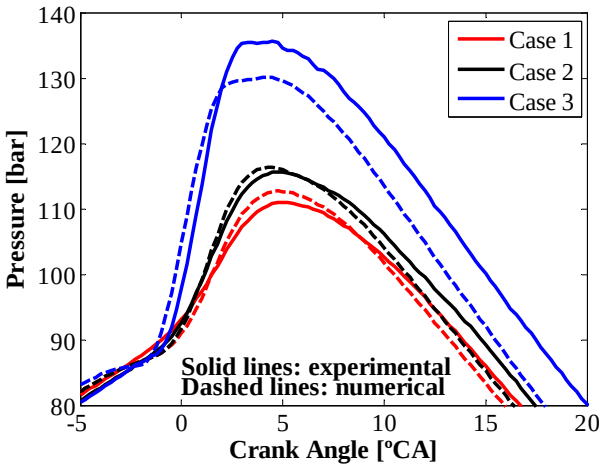

Figure 12 – Comparison between simulated and experimental pressure traces for Cases 1-3.

The standard heat release calculation method [4], taking into account heat transfer to the walls, was applied to the experimental and simulated pressure traces in order to determine apparent GHRR. Figure 13 compares the simulated and experimental results of the apparent GHRR for Cases 1-3. In general, the peak GHRR and the shape of the traces are well predicted for all cases. This result is expected because of the minor role of turbulence and mixing between zones during the main heat release event in HCCI engines, particularly when combustion phasing is close to TDC. Similar results have been observed in previous research using 40 zones and KIVA-3V as the CFD code. It is particularly important to note in Figure 12 and 13 that the peak pressure rise and peak heat release rate are well predicted by the 12-zone reduced model, therefore allowing accurate predictions of ringing intensity in comparison with prior modeling approaches.

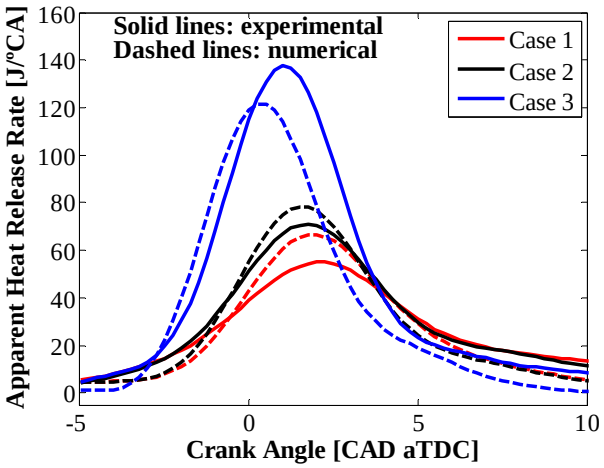

Figure 13 – Comparison between simulated and experimental apparent gross heat release rates for Cases 1-3.

Cases 4-6 evaluate the reliability of the 12-zone reduced model when delayed combustion is used to increase the power output and reduce the ringing intensity. From Table 3, the IMEP in Case 5 is close to 9 bar, which represents almost 70% of the achievable power output for the Diesel version of the VW engine used in the experiments. Furthermore, the operating conditions in Case 5 reduce the average ringing intensity by 50% when compared with Case 3. Figure 14 shows a comparison between experimental and simulated pressure traces for Cases 4-6. In Cases 4 and 5 the peak pressure and the shape of the pressure trace are reasonably well predicted by the model. However, for Case 6 the accuracy of the model is reduced because of the increased importance of mixing between zones on heat release rates. For Cases 4 and 5 the differences observed between experimental and computed results in the onset of combustion could be due to the temperatures at IVC being calculated using average CHR from 300 cycles instead of CHR for the representative cycle. For Case 6, the errors in the model predictions are explained by the increased experimental cycle-to-cycle variations at delayed combustion that lead to higher uncertainties in determining the initial conditions at IVC. As mentioned before, the experimental data

was recorded during multi-cylinder operation, at a relatively high engine speed, and for a high octane fuel. These conditions combined with highly delayed combustion (Case 6) make it difficult to achieve reliable experimental data because the range of HCCI stable operation is narrower at lower residence times and for fuels with higher autoignition temperature [14]. As a result, the intake conditions can be affected by cyclic variations, including further variability between cylinders.

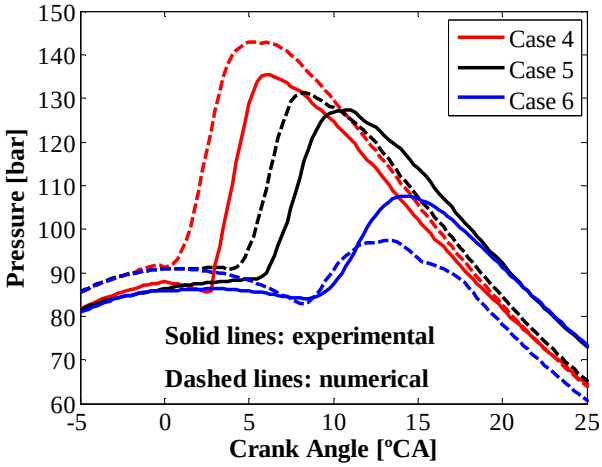

Figure 14 - Comparison between simulated and experimental pressure traces for Case 4-6.

Figure 15 shows the simulated and experimental traces of apparent GHRR for Cases 4-6. In general, the model makes good predictions of shape and peak GHRR. The model also predicts the experimental trends for differences in the peak of the GHRR, the combustion phasing, and the burn duration between different cases. The prediction of these combustion variables allows the model to predict the decrease in the peak pressure rise rates and consequently the decrease in ringing intensity with delayed combustion phasing, which is observed in the experiments. For Case 6, the GHRR is more likely to be influenced by mixing between zones and cyclic variability. As a result the difference between the experimental and simulated peak of the GHRR is higher, as well as the difference in the shape of the traces.

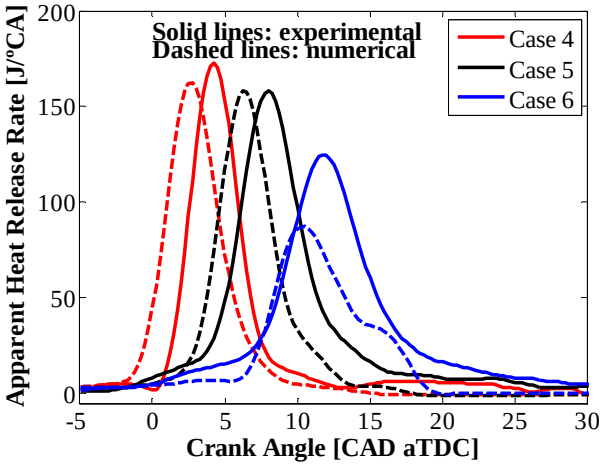

Figure 15 – Comparison between simulated and experimental pressure traces for Cases 4-6.

Fig. 16 shows the ratio of calculated vs. experimental combustion and emissions parameters. Exhaust emissions are calculated at EVO. NO_x emissions are not included in the analysis because the experimental and simulated values were generally below 20 ppm. In general, the predictions of the 12-zone reduced model are reasonably good for $IMEP_g$, gross indicated efficiency, individual ringing intensity, burn duration, and HC emissions. Although not shown in Fig. 16, the trends experimentally observed for the mentioned

variables with changes in equivalence ratio or intake temperature were also generally well predicted. For Case 6 (most delayed combustion) the prediction of ringing intensity and HC emissions are poor because of the high sensitivity to cyclic variability and mixing between zones. Delaying combustion to enable higher power output is usually accompanied by a decrease in intake temperature and an increase in equivalence ratio. The combination of these strategies causes more sensitivity of the autoignition process and heat release to changes in charge and residual temperature, turbulence, and heat transfer. As a result, with excessively delayed combustion timing more cycles tend to misfire and other cycles tend to produce high peak pressure rise rates. Therefore, the prediction of variables like ringing intensity and HC emissions becomes more difficult for a model based on single cycle calculations.

CO emissions are substantially underpredicted for all cases because these emissions are very difficult to predict with the methodology proposed here, which does not allow for mixing between zones. Similar results for CO emissions have been achieved for other sequential CFD/detailed chemical kinetics models even using more zones (40). CO emissions originate from poor CO-to-CO_2 oxidation, which typically occurs below 1500 K. From the temperature profile shown in Fig. 10, which is typical for Cases 3-6, it is observed that the zones located in the core and boundary layer usually exhibit peak temperatures higher than 1500 K; therefore, almost all the CO produced in these zones is oxidized to CO_2. Since the peak temperature of zones located in the boundary layer is highly sensitive to the EHTAF, this parameter can be tuned to allow better predictions of CO emissions. In this research, the CO emissions were reasonably well predicted when the peak temperature of zones located in the boundary layer were enforced to be within a range of 1200-1400K by setting the EHTAF. These predictions are not presented in Fig. 16 because different values for the EHTAF were used in the zones located in the boundary layer. From previous studies it is concluded that at high loads the major sources of CO and HC emissions are the crevices and the boundary layer near the wall [7, 28], and at low equivalence ratios the major source of these emissions is the incomplete oxidation of the bulk gas [28-30]. This variability in the main source of these emissions with changing equivalence ratios makes it difficult to define a recommended heat transfer scheme to accurately predict the CO and HC emissions for all loads. Therefore, it is necessary to run parametric studies to identify the recommended heat transfer scheme in order to allow better predictions of CO emissions without affecting the prediction of HC emissions.

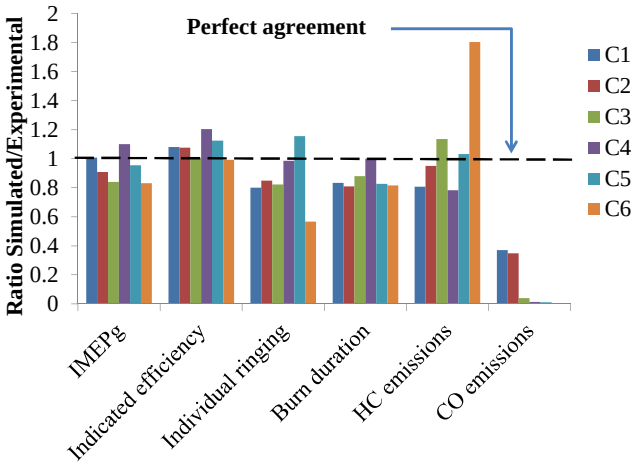

Figure 16 – Ratio of Simulated-over-experimental results for Cases 1-6 (C1-C6). Experimental results are extracted from Table 3. HC and CO emissions are calculated at EVO.

CONCLUSIONS

A new sequential Chemical Kinetics-CFD-Chemical Kinetics methodology is proposed to predict combustion characteristics and the main emissions from HCCI engines. The proposed methodology follows three steps: 1) a 1-zone model (Chemkin Pro) using detailed chemical kinetics is run to predict either the IVC conditions to achieve a desired combustion timing, or the combustion timing achieved with given IVC conditions. This first step also determines the energy switch crank angle where multi-zone kinetic calculations start. 2) CFD simulations are performed (Fluent 6.3) at motored conditions to define the number of zones that allows good resolution of thermal stratification (40 zones in this research), the mass fraction in each zone, and the temperature history based on the average zone temperature calculated within a specific crank angle interval. Finally, 3) The temperature profile for each zone is specified in a multi-zone chemical kinetic model (Chemkin Pro) using the energy switch time defined earlier. In this final step, detailed combustion and emissions parameters are determined.

A technique for significantly reducing the number of zones in the multi-zone simulation step is discussed. This method allows significant reduction in computing time while still maintaining accuracy in calculating the main combustion parameters and emissions. Zone reduction is performed by grouping the zones that remain non-reacted at adiabatic conditions into a single zone. The reduced number of zones and the temperature and mass fraction profiles for each zone are fed into the multi-zone model of Chemkin Pro to calculate HCCI combustion characteristics using detailed chemical kinetics. The result of the modeling process is a 12-zone reduced model which preserves the resolution of the original 40-zones model.

The model is validated against experimental results achieved on a multi-cylinder engine using biogas as a fuel for six different points of operation. The $IMEP_g$, indicated efficiency, individual ringing intensity, burn duration, NO_x and HC emissions are reasonably well predicted. The prediction of CO emissions is generally poor, but it is highly improved when heat transfer from boundary layer zones is adjusted to produce zone peak temperatures between 1200-1400K.

The new methodology allows for a better understanding of the effect of number of zones on the resolution of thermal and mass in-homogeneities, as well as good estimation of main HCCI combustion characteristics and emissions with reduced computing time. It is particularly important to note that the newly proposed 12-zone reduced model allows more accurate predictions of peak pressure rise rates and ringing intensity.

REFERENCES

1. Najt, P. M., and Foster, D. E., "Compression Ignited Homogeneous Charge Combustion", *SAE Paper 830264*, 1984, doi: 10.4271/830264.
2. Richter, M., Franke, A., Alden, M., Hultqvist, A., and Johansson, B., "Optical Diagnostics Applied to a Naturally Aspirated Homogeneous Charge Compression Ignition Engine". *SAE Paper 1999-01-3649*, 1999, doi: 10.4271/1999-01-3649.
3. Hultqvist, A., Christensen, M., Johansson, B., Franke, A., Richter, M., and Aldén, M., "A Study of the Homogeneous Charge Compression Ignition Combustion Process by Chemiluminescence Imaging", *SAE Paper 1999-01-3680*, 1999, doi: 10.4271/1999-01-3680.
4. Heywood, J. B., "Internal Combustion Engine Fundamentals", McGraw-Hill, New York, ISBN-13: 978-0070286375, p. 930, 1988.
5. Aceves, S. M., Flowers, D. L., Westbrook, C. K., Smith, J. R., Pitz, W., Dibble, R., Christensen, M., and Johansson, B., "A Multi-Zone Model for Prediction of HCCI Combustion and Emissions", *SAE Paper 2000-01-0327*, 2000, doi: 10.4271/2000-01-0327.
6. Aceves, S. M., Flowers, D. L., Martinez-Frias, J., Smith, J. R., Westbrook, C. K., Pitz, W. J., Dibble, R., Wright, J. F., Akinyemi, W. C., and Hessel, R. P., "A Sequential Fluid-Mechanic Chemical-Kinetic Model of Propane HCCI Combustion", *SAE Paper 2001-01-1027*, 2001, doi: 10.4271/2001-01-1027.
7. Aceves, S. M., Flowers, D. L., Espinosa-Loza, F., Martinez-Frias, J., Dibble, R. W., Christensen, M., Johansson, B., and Hessel, R. P., "Piston-Liner Crevice Geometry Effect on HCCI Combustion by Multi-Zone Analysis", *SAE Paper 2002-01-2869*, 2002, doi: 10.4271/2002-01-2869.
8. Flowers, D. L., Aceves, S. M., Martinez-Frias, J., and Dibble, R. W., "Prediction of carbon monoxide and hydrocarbon emissions in iso-octane HCCI engine combustion using multizone simulations", *Proceedings of the Combustion Institute*, 29(1): 687-694. 2002, doi: 10.1016/S1540-7489(02)80088-8.
9. Aceves, S. M., Flowers, D. L., Martinez-Frias, J., Espinosa-Loza, F., Christensen, M., Johansson, B., and Hessel, R. P., "Analysis of the Effect of Geometry Generated Turbulence on HCCI Combustion by Multi-Zone Modeling", *SAE Paper 2005-01-2134*, 2005, doi: 10.4271/2005-01-2134.
10. Flowers, D. L., Aceves, S. M., Martinez-Frias, J.,Hessel, R., and Dibble, R. W., "Effect of Mixing on Hydrocarbon and Carbon Monoxide Emissions Prediction for Isooctane HCCI Engine Combustion Using a Multi-zone Detailed Kinetics Solver", *SAE Paper 2003-01-1821*, 2003, doi: 10.4271/2003-01-1821.
11. Aceves, S. M., Flowers, D. L., Espinosa-Loza, F., Babajimopoulus, A., and Assanis, D.N., "Analysis of Premixed Charge Compression Ignition Combustion with a Sequential Fluid Mechanics-Multizone Chemical Kinetics Model", SAE Paper 2005-01-0115, 2005, doi: 10.4271/2005-01-0115.
12. Cao, L., Bhave, A., Su, H., Mosbach, S., Kraft, M., Dris, A., and McDavid, R., "Influence of Injection Timing and Piston Bowl Geometry on PCCI Combustion and Emissions", *SAE Paper 2009-01-1102*, 2009, doi: 10.4271/2009-01-1102.
13. Zhao, H., "HCCI and CAI Engines for the Automotive Industry", Wood head Publishing Ltd, Cambridge, ISBN-10: 1845691288, p. 544, 2007.
14. Shahbakhti, M., and Koch, C. R., "Characterizing the cyclic variability of ignition timing in a homogeneous charge compression ignition engine fuelled with n-heptane/iso-octane blend fuels", *International Journal of Engine Research*, 9: 361-397, 2008, doi: 10.1243/14680874JER01408.
15. Saxena, S., Chen, J-Y, and Dibble, R., "Maximizing Power Output in an Automotive Scale Multi-Cylinder Homogeneous Charge Compression Ignition (HCCI) Engine", SAE Paper 2011-01-0907, doi: 10.4271/2011-01-0907.

16. Smith, Gregory P., Golden David M., Frenklach, Michael., Moriarty, Nigel W., Eiteneer, Boris., Goldenberg, Mikhail., Bowman, C. Thomas., Hanson, Ronald K., Song, Soonho., Gardiner Jr, William C., Lissianski, Vitali V., and Qin, Z. (n.d.). "GRI-Mech 3.0", *http://www.me.berkeley.edu/gri-mech/*, Aug. 2011.
17. Petersen, E. L., Davidson, D. F., and Hanson, R. K., "Ignition Delay Times of Ram Accelerator CH_4/O_2/ Diluent Mixtures", Journal of Propulsion and Power, 15(1): 82-91, 1999.
18. Agarwal, A., and Assanis, D.N., "Multi-Dimensional Modeling of Natural Gas Ignition Under Compression Ignition Conditions Using Detailed Chemistry", *SAE Paper 980136*, 1998, doi: 10.4271/980136.
19. Agarwal, A., and Assanis, D.N., "Modeling the Effect of Natural Gas Composition on Ignition Delay Under Compression Ignition Conditions", *SAE Paper 971711*, 1997, doi: 10.4271/971711.
20. Sjöberg, M., and Dec, J. E., "An investigation of the relationship between measured intake temperature, BDC temperature, and combustion phasing for premixed and DI HCCI engines", *SAE Paper 2004-01-1900*, 2004, doi: 10.4271/2004-01-1900.
21. Woschni, G., "Universally Applicable Equation for the Instantaneous Heat Transfer Coefficient in the Internal Combustion Engine", *SAE Paper 670931*, 1967, doi: 10.4271/670931.
22. Soyhan, H. S., Yasar, H., Walmsley, H., Head, B., Kalghatgi, G. T., and Sorusbay, C., "Evaluation of heat transfer correlations for HCCI engine modeling", *Applied Thermal Engineering*, 29(2-3): 541-549, 2009, doi: 10.1016/j.applthermaleng.2008.03.014.
23. Chang, J., Güralp, O., Filipi, Z., Assanis, D., Kuo, T.-W., Najt, P., and Rask, R., "New Heat Transfer Correlation for an HCCI Engine Derived from Measurements of Instantaneous Surface Heat Flux", *SAE Paper 2004-01-2996*, 2004, doi: 10.4271/2004-01-2996.
24. Bedoya, I. D., Saxena, S., Cadavid, F. J., Dibble, R. W., and Wissink, M., "Experimental study of biogas combustion in an HCCI engine for power generation with high indicated efficiency and ultra-low NOx emissions", *Energy Conversion and Management*, 52(1): 154-162, 2012, doi: 10.1016/j.enconman.2011.08.016.
25. Bedoya, I. D., Saxena, S., Cadavid, F. J., Dibble, R. W., and Wissink, M., "Experimental evaluation of strategies to increase the operation range of a biogas HCCI engine for power generation", presented at Third International Conference on Applied Energy-ICAE2011, Perugia, Italy, May 16-18, 2011, 2219-2244.
26. Eng, J. A., "Characterization of Pressure Waves in HCCI Combustion", *SAE Paper 2002-01-2859*, 2002, doi: 10.4271/2002-01-2859.
27. Savitzky, A., and Golay, M. J. E., "Smoothing and differentiation by simplified least-squares procedures." *Analytical Chemistry*, 36(8): 1627-1639, 1964, doi: 10.1021/ac60214a047.
28. Dec, J. E., Sjöberg, M., Hwang, W., Davisson, M. L., and Leif, R. N., "Detailed HCCI Exhaust Speciation and the Sources of Hydrocarbon and Oxygenated Hydrocarbon Emissions", *SAE Paper 2008-01-0053*, 2008, doi: 10.4271/2008-01-0053.
29. Sjöberg, M., and Dec, J. E., "Combined Effects of Fuel-type and Engine Speed on Intake Temperature Requirements and Completeness of Bulk-gas Reactions for HCCI Combustion", *SAE Paper 2003-01-3173*, 2003, doi: 10.4271/2003-01-3173.
30. Sjoberg, M., and Dec, J. E., "An investigation into lowest acceptable combustion temperatures for hydrocarbon fuels in HCCI engines", *Proceedings of the Combustion Institute*, 30(2): 2719-2726, 2005, doi: 10.1016/j.proci.2004.08.132.

CONTACT INFORMATION

Corresponding author: Iván D. Bedoya

Department of Mechanical Engineering

Grupo de Ciencia y Tecnología del Gas y Uso Racional de la Energía

University of Antioquia, Medellín, Colombia

E-mail address: ibedoyac@udea.edu.co

Tel: +57 4 2198548; fax: +57 4 263 8282

ACKNOWLEDGMENTS

The authors express thanks to the following institutions for giving financial support to the Colombian research project: "Estudio del Uso de Motores de Encendido por Compresión de Carga Homogénea (HCCI) en la Valorización del Biogás para Generación de Electricidad":

University of California, Berkeley.

Departamento Administrativo de Ciencia, Tecnología e Innovación COLCIENCIAS - Colombia.

Servicio Nacional de Aprendizaje SENA - Colombia.

University of Antioquia - Colombia.

The Natural Sciences and Engineering Research Council of Canada through the Canada Graduate and PostGraduate Scholarship Programs.

US DOE Advanced Engine Consortium (AEC/HCCI).

DEFINITIONS/ABBREVIATIONS

aTDC	After top dead center
CAxx	Crank angle for x% heat release (i.e. CA50 = Crank angle for 50% heat release as CAD ATDC)
CAD	Crank angle degree
CFD	Computational Fluid Dynamics
CHR	Cumulative heat release
EVC	Exhaust valve close
EVO	Exhaust valve open
EHTAF	External heat transfer area fraction
GHRR	Gross heat release rate
HCCI	Homogeneous Charge Compression Ignition
HCT	Hydrodynamics, chemistry and transport
$IMEP_g$	Gross indicated mean effective pressure
IVC	Intake valve close
IVO	Intake valve open
PCCI	Premixed charge compression ignition
PM	Particulate matter
TDC	Top dead center
ϕ (phi)	Equivalence ratio